Available online at www.sciencedirect.com
SCIENCE DIRECT®
International Journal of Multiphase Flow 31 (2005) 643–665
International Journal of Multiphase Flow
www.elsevier.com/locate/ijmulflow

Dynamics of two-phase downwards flows in submerged entry nozzles and its influence on the two-phase flow in the mold

A. Ramos-Banderas, R.D. Morales *, R. Sánchez-Pérez, L. García-Demedices, G. Solorio-Diaz

Department of Metallurgy and Materials Engineering, IPN-ESIQIE, Apdo. Postal 75-874, D.F., CP 07338, Mexico

Received 3 March 2004; received in revised form 3 January 2005

Abstract

Gas–liquid flows inside the submerged entry nozzle (SEN) of a slab mold and its influence in the flow field in the mold were studied using video recording, mathematical simulations and particle image velocimetry (PIV) approaches. Bubbly and annular flows in the SEN yield structurally-uncoupled and structurally coupled flows in mold, respectively. High gas loads (ratio of mass flux of gas and mass flux of liquid) at high casting rates lead to increases of bubble population and bubbles sizes due to coalescence processes whose rate exceeds that of their breakup. The presence of gas bubbles or gas layers inside the SEN lead to periodical twisting of the liquid flow that induces biased flows through both ports yielding uneven flows in the mold. A multiphase mathematical model predicts acceptably well the flow dynamics of two-phase flows inside the SEN.

Keywords: Two-phase flows; SEN; Mold; Continuous casting; Bubbles; PIV

* Corresponding author. Tel./fax: +52 55 5729 6000.
E-mail addresses: rmorales@ipn.mx, ketechnologies@prodigy.net.mx (R.D. Morales).

0301-9322/$ - see front matter © 2005 Elsevier Ltd. All rights reserved.
doi:10.1016/j.ijmultiphaseflow.2005.01.010

1. Introduction

Dynamics of two-phase downwards flows has a high relevance in submerged entry nozzles (SEN) of continuous casting molds of steel. Through the SEN liquid steel is fed into the mold together with argon gas whose function is to avoid the excessive deposit of solid alumina particles (produced by the reaction between dissolved oxygen and aluminum in steel) on the exit ports. Supposedly argon drags those particles into the mold avoiding SEN clogging. However, as seen in Fig. 1, molten steel entering the mold may carry inclusion particles (alumina, silicates, etc.) and drags argon bubbles, as reported by Yuan et al. (2003), which can be trapped in the solid shell. Moreover, liquid flux, on the top of the bath, can also be entrained by the shear of liquid flow across the top surface, forming large harmful inclusions in solidified steel. These inclusions and bubbles will either be safely transported to the top surface and removed by the slag layer or become entrapped in the shell, at the solid/liquid interface of the solidifying metal. Fluid flows in continuous casting systems are highly turbulent and consequently unsteady and fluctuating producing an uneven and asymmetrical distribution of defects in the slab of steel. Sánchez-Pérez et al. (2004) studied the two-phase flow, steel–argon, in a slab mold, and defined quantitatively the tran-

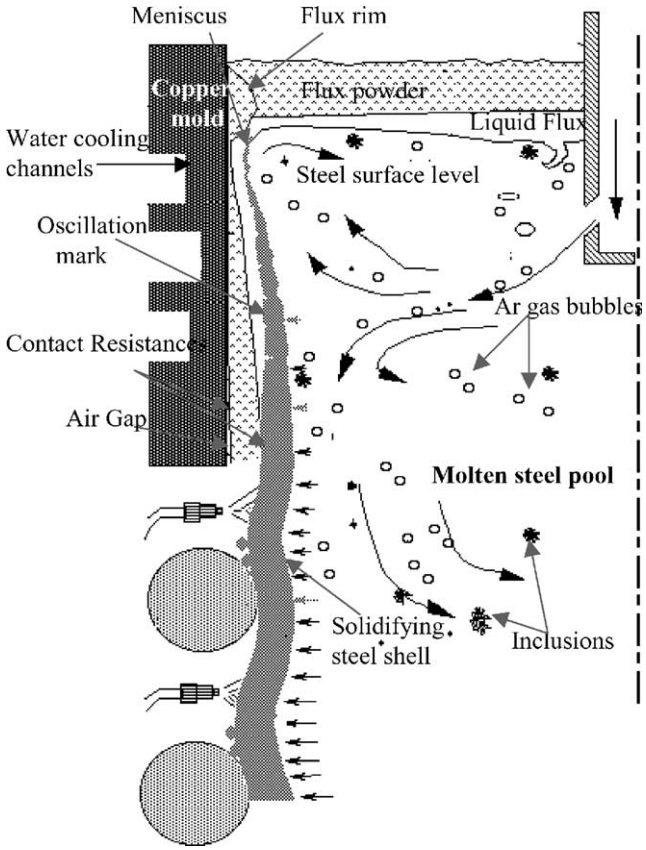

Fig. 1. Schematic of multiphase flow in the mold (after Yuan et al. (2003)).

sition between structurally uncoupled and structurally coupled flows determined through particle image velocimetry measurements and mathematical simulation approaches using a water model. The second type of flows is that where the path lines of both phases observe similar structures. Transition is basically governed by the ratio between the drag forces exerted by the liquid on gas bubbles and the inertial forces of liquid. This ratio is function itself of the gas load (ratio of mass flow rate of gas and mass flow rate of liquid) in the SEN. In another paper, Sánchez-Pérez et al. (2003), using again a water model, found that the two-phase flow exiting from the SEN is divided into a bubble jet and a liquid jet where gas is the majority and minority phase, respectively. The angles of both jets, with regard the horizontal line, are dependent on the gas load and the casting speed. They found also that the volume of liquid entrained by bubbles toward the top surface exhibits an exponential growth with the gas load. On the other hand, efforts to decrease flow turbulence through the dissipation of the kinetic energy using swirling jets, from the SEN ports, have been reported by Yokoya et al. (1998, 2000a), who employed also water models and mathematical simulations for one-phase flows. The swirl flow is originated by a blade located inside the SEN and they found that increases of the tangential velocity originate decreases of the axial velocity in the axis of the SEN. By changing the swirl strength it is possible to control the flow pattern and the direction of the flow. Yokoya et al. (2000b, 2001), also reported that using the swirling jet the bath oscillations decreased as a result of a decreasing of flow turbulence in a slab mold. However, these authors have not considered the swirling effects on two-phase flows.

A complete review of fluid flow simulation in continuous casting molds has been published by Thomas and Zhang (2001), and works related with the specific two-phase flow in the SEN are rather scarce. Burty et al. (1995) employed a water–air model to define bubbly and annular domains for different gas loads as functions of Froude number of both phases. In the same work they extrapolated their results to interpret actual argon–liquid steel flows affecting the Froude number of the gas phase by the ratio of densities between steel and water defining also domains for bubbly and annular flows. Using a water model Thomas et al. (1997), studied the flow dynamics of bubbly flows in a SEN finding the relationship between gas injection rate, gas injection pore diameter and the average diameter of bubbles. Probably the most complete contributions, so far, regarding the dynamics of two-phase flows in SEN's, are those of Bai and Thomas (2001a,b,c). In the first work these authors employed an Eulerian multiphase model to simulate two-phase turbulent flow of liquid steel and argon bubbles in a slide gate nozzle and validated the results through PIV measurements. They reported a gas rich jet with a small downward angle but this is the opposite of that found by Sánchez-Pérez et al. (2003, 2004), who reported a downward gas rich jet with a large downward angle and above of it a liquid rich jet using PIV measurements in a water model. In the second and third papers of Bai and Thomas they reported that the degree of the sliding valve opening originates the biased flow of liquid and gas through the SEN's ports. Accordingly, large bubbles cause a shallower jet angle and large flow fluctuations in the mold. Larger bubbles tend to reduce the backflow zone in the exit port but enhance turbulence especially at high gas loads. The bubble size increases and the size distribution become less uniform as the liquid velocity and gas flow rate increase. All those later results are in agreement with the experimental findings of Sánchez-Pérez et al. (2003, 2004). Bai and Thomas also found that the deposits of alumina particles inside the SEN contribute strongly to the biased flow of steel and argon through the ports of the SEN. The same authors, Bai and Thomas (2001d), developed a simple but ingenious mathematical model of bubbly flow in a SEN using the results of a water model.

Their model estimates the sizes of bubbles as functions of gas load and the bore size of the gas injectors.

In actual liquid steel–argon gas flows in contact with a SEN made of a refractory-ceramic material the contact angle between steel and the SEN wall is high. That is, steel does not wet the wall of a SEN. This effect has been taken into account in the work of Wang et al. (1999), using a SEN made of plastic with interior walls covered with wax. They found that when water does not wet the wall immediate detachment of bubbles is promoted. Bath level oscillation, for the same gas load, is increased under non-wetting conditions. Similar findings are reported for porous gas injectors when wetting and non-wetting materials are used as reported by Mizuno and Iguchi (2001). More recently Ishiguro and Iguchi (2003), used a SEN made of plastic with interior walls covered with wax and studied, via image analysis of photos, the two-phase downwards flow of water and air. They established stability maps for film, bubbly, bubbly-slug, slug-annular, annular and slug flows using the superficial velocities of both phases in the column.

In the present work we emphasize the importance of the two-phase flow regime in the SEN as well as its important influence on the fluid flow patterns inside the mold. Furthermore, the unsteady nature of the fluid flow and the distribution of the volume fractions of both phases, which are not considered in previous works, are also analyzed. The final aim is to contribute with additional knowledge to the complex and important two-phase flow in continuous casting systems.

2. Experimental methods and mathematical model

2.1. Experimental apparatus of two-phase flows in the mold

A 1/2 scale model of IMEXSA Steel (located in Lazaro Cárdenas Michoacán, Mexico) mold was built using 20 mm thick transparent plastic sheets; the geometric dimensions are shown in Fig. 2(a). Water is delivered through a SEN (see Fig. 2(b)) with a conventional design. At this step the effects of the slide gate opening or its orientation are not considered. Flow rate of water into the mold model is controlled by globe valves and flow meters and is drained through a honeycomb type plate located in the bottom. The outer water is sent back to a storage tank to be re-circulated into the mold. Injection of air, from a compressor, into the SEN is performed using a connection and a gas flow meter to feed, accurately, different flow rates of this gas. Air was introduced into the SEN through a central pipe ($\Phi = 3.75$ mm) located in the upper SEN body. This pipe is fed by through a duct ($\Phi = 5$ mm) duct which receives air from the compressor line. Bubbly flows were recorded by a fast video camera. Dimensions of the SEN are shown in Fig. 2(b).

Fluid dynamics under different operating conditions was characterized through particle image velocimetry (PIV) technique using equipment from Dantec Systems. A green frequency double pulsed Nd:YAG laser with a wavelength of 532 nm was employed. In order to obtain short bursts of light energy, the lasing cavity is Q-switched so that the energy is emitted in 6–10 ns bursts opposed to pulses of 250 μs, which is the duration of the exciting lamp in the laser cavity. Output energy from the laser is 20 mJ of Nd:YAG crystal from the fiber bundle. This energy is increased with light guides that can transmit 500 mJ of pulsed radiation with an optical transmission that is greater than 90% at 532 nm. Interrogation areas of 0.432×0.261 m in the flow were scanned with a resolution of 32×32 or 64×64 pixels.

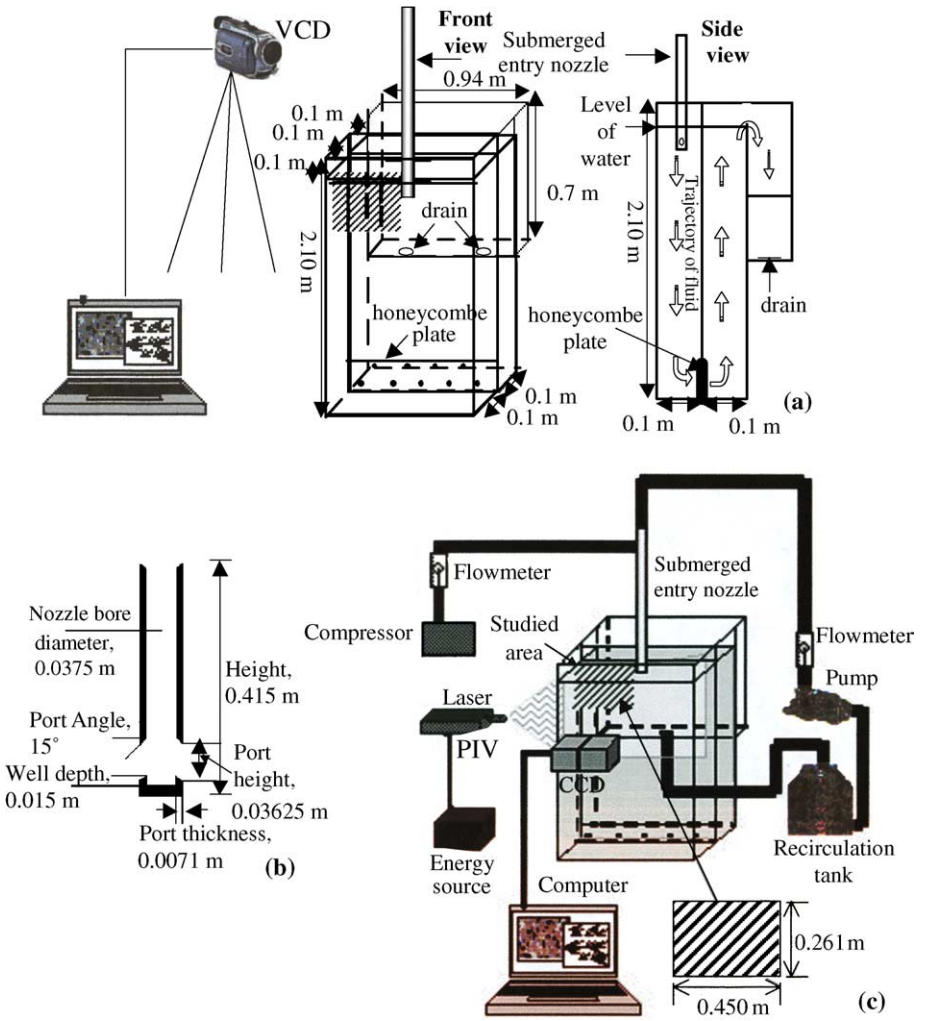

Fig. 2. (a) Geometric dimensions of the experimental model, (b) SEN and (c) scheme of the experimental set-up.

The laser sheet is 0.001 m thick and it was positioned at half the mold thickness by means of a computer-controlled frame-holder system with 3-D motions; this plane includes from the SEN axis to one of the narrow walls of the mold. In order to follow the fluid flow the fluid was previously seeded with polyamide particles with a density of 1030 kg/m^3 and an uniform size of 20 μm, which were injected in the SEN. A cross-correlation procedure using fast Fourier transforms allowed processing the recorded signals and a Gaussian distribution function was used to determine the location of the maximum of the peak displacement with sub-pixel accuracy (Odenthal et al., 2002). The signals were recorded by a Dantec coupled charged device (CCD) with 90 mm Nikon lenses and the recordings were processed using commercial Flow Map software in a Pentium-IV PC in order to obtain the vector–velocity fields. To record the flow fields of air in the bubbles two CCD's were mounted in a twin holder fixed to the frame-holder system. The first CCD captured

the images from the laser sheet and transferred them to the other parallel CCD through a prism. In the second CCD there is a red filter, to avoid the passage of green light. This filter allowed the detection and recording of air flow velocity fields by masking the vectors of the liquid phase. Fig. 2(c) is a scheme of the experimental set-up.

One hundred images for each experiment and for each phase flow fields were analyzed using this procedure. Vorticity fields of the flow patterns were derived from the velocity fields, as determined by the PIV measurements, using a finite center difference scheme,

$$\omega_k = \frac{\partial u_i}{\partial x_j} - \frac{\partial u_j}{\partial x_i} \tag{1}$$

Bubble sizes were calculated from the video images captured by the CCD's, which were recorded in a PC, calculation of bubble sizes and their population was performed using commercial software of image analysis. This is an image analyzer program which uses mathematical filters and combinations of contrast, brightness and zooms which make possible the resolution, definition and identification of individual bubbles or groups of agglomerated bubbles in mist type flows. From the 100 images for each case, 35 were randomly chosen for bubble analysis; this means that in the case of the highest and lowest mass loads about 300 000 and 75 000 bubbles were analyzed, respectively. The information stored for all these experiments totalized about 20 GB.

The experimental program, including the experimental gas loads, is shown in Table 1 where SI and more conventional units are shown; the casting speed was employed as the scaling up criterion, and thus the same casting speeds used in the casting plant were employed in the model because this procedure allows an intermediate criterion between full scale Reynolds modeling and Froude criterion. The main experimental variables include casting speed and gas flow rate or gas-load.

2.2. Mathematical model

Two-phase flow inside the SEN, including only bubbly flows, was simulated using the VOF (volume of fluid) model. In the VOF model (Hirt and Nichols, 1981), a single set of momentum

Table 1
Experimental conditions for model experiments

Parameter		Value				
Gas flow rate $\times 10^5$, m^3/s		0.833, 2.0, 4.17, 8.33, 16.70				
Gas flow rate, l/min		0.5, 1.2, 2.5, 5.0, 10.0				
Casting speed, m/min		0.8, 1.2, 1.8				
Water flow rate, l/min		80, 120, 160				
Gas-load $\times 10^5$	Water flow rate, l/min	Gas flow rate, l/min				
		0.5	1.2	2.5	5.0	10.0
	80	0.62 (B)	0.88 (B)	3.20 (B)	6.76 (A)	15.82 (A)
	120	0.55 (B)	0.89 (B)	2.22 (B)	4.15 (A)	7.89 (A)
	160	0.32 (B)	0.69 (B)	1.02 (B)	3.39 (A)	6.93 (A)

(A) Annular flow; (B) bubbly flow.

equations is shared by the two fluids and the volume fraction of the fluids is tracked throughout the domain. The gas–liquid interface between air bubbles and water is treated as a movable pressure boundary. The tracking of the interface is accomplished by the solution of an unsteady continuity equation for the volume fraction of both phases,

$$\frac{\partial \alpha_q}{\partial t} + u_j \frac{\partial \alpha_q}{\partial x_i} = S_v \tag{2}$$

where α_q is the volume fraction of phase "q" and S_v is the source term. The momentum transfer equations for the tow-phase flows are,

$$\frac{\partial}{\partial t}\rho u_j + \frac{\partial}{\partial x_i}\rho u_i u_j = -\frac{\partial p}{\partial x_j} + \frac{\partial}{\partial x_i}\left[\mu_{\text{eff}}\left(\frac{\partial u_i}{\partial x_j} + \frac{\partial u_j}{\partial x_i}\right)\right] + \rho g_j \tag{3}$$

where μ_{eff} is the effective dynamic viscosity of the continuous phase. The averaged density and viscosity of the mixture are given by,

$$\rho = \alpha_{\text{l}}\rho_{\text{l}} + \alpha_{\text{g}}\rho_{\text{g}} = \bar{\rho}_{\text{l}} + \bar{\rho}_{\text{g}} \tag{4}$$

$$\mu = \alpha_{\text{l}}\mu_{\text{l}} + \alpha_{\text{g}}\mu_{\text{g}} = \bar{\mu}_{\text{l}} + \bar{\mu}_{\text{g}} \tag{5}$$

This system has a constraint given by

$$\alpha_{\text{l}} + \alpha_{\text{g}} = 1 \tag{6}$$

To simplify the calculations here the well known k–ε model of turbulence of Launder and Spalding (1974) was employed using the corresponding equations for the turbulent kinetic energy k and its dissipation rate ε.

The local curvature of the gas region, defined by the radius of curvature R, is related to the pressure difference at the gas–liquid interface according to Laplace–Young equation

$$p_{\text{b}} - p = \frac{2\sigma}{R} \tag{7}$$

Gas expansion in the gas bubble was estimated assuming an isothermal process. Superficial tension of water in the model is 0.072 Nw/m. Boundary conditions such as no-slipping on solid surfaces, and the wall law for cells close to solid surfaces were all standard in agreement to the k–ε model. For the boundary condition of kinetic energy of the liquid at the inlet a flat velocity profile is assumed just before the entrance of the gas inlet. This velocity corresponds to the flow rate of water divided by the cross section area of the SEN. Then the kinetic energy at the entry is $k = (3/2)(0.0073)u^2$ and the dissipation rate of kinetic energy at the inlet would be $\varepsilon = k^{1.5}/C_{\mu}^{0.25}R_{\text{s}}$ where C_{μ} is a constant of the turbulence model and R_{s} is the internal radius of the SEN.

The computing technique involved the use of finite volume techniques in its finite differences version so that no coordinate changes of the physical domain were required. The SIMPLEC algorithm (Chung, 2002) PISO integrated in the CFD 2000 code was employed because of its good performance to find a fast converged solution. These equations are solved using and explicit time-marching scheme applying a multistage time step of the volume fraction equations. Refinement of the time step is attained through the Courant's condition (Hoffmann, 1989). A user

defined subroutine was built for the VOF model. The criterion of numerical convergence was that when all residuals of all the flow variables decreased to values smaller than 1×10^{-5}. All the simulations were run in a Silicon Graphics Workstation at the Laboratory of Mathematical Simulations of Materials Processing and Fluid Dynamics of IPN-ESIQIE.

3. Results and discussion

3.1. Structurally-uncoupled and structurally-coupled flows in the mold

In the work of Sánchez-Pérez et al. (2004), the authors classified, on basis of measured maps of streamlines of both phases, what is called structurally-uncoupled and structurally-coupled flows (see Fig. 9(a)–(d) of this reference). A structurally-coupled flow is that where the streamlines of the liquid and gas phases observe high similarities. The transition between structurally-uncoupled and structurally-coupled flows depends on the relationship between the dimensionless parameters of the mass flux ratio or gas load and the pi-momentum given by the expression,

$$\Pi_{\text{mom}} = \frac{\tau_{\text{g}}}{\tau_{\text{l}}} = \frac{\bar{\rho}_{\text{g}} L}{\bar{\rho}_{\text{l}} u \tau_v} \left(1 - \frac{v}{u}\right) \tag{8}$$

where L is the jet length, u and v are the velocities of the liquid and gas phases, measured through the determinations of velocities with the PIV respectively; τ_v is the time response of the dispersed phase (gas bubbles) to the disturbs coming from the continuous phase (water) and is given by,

$$\tau_v = \frac{\rho_{\text{g}} d_{\text{b}}^2}{18\mu} \tag{9}$$

where d_{b} is the bubble size measured from the videos taken by the CCD and using the image analyzer, the gas load is defined in this work as,

$$M_{\text{L}} = \frac{\bar{\rho}_{\text{g}} v}{\bar{\rho}_{\text{l}} u} \tag{10}$$

$\bar{\rho}_{\text{g}}$ and $\bar{\rho}_{\text{l}}$ are given by the terms in Eq. (4). Parameter Π_{mom} in Eq. (8) is the ratio between the drag momentum transfer exerted by the liquid on the bubbles surfaces and the inertial momentum transfer of the fluid. When this parameter exceeds the value of 1.6×10^{-5} approximately, the flow enters into a transition zone and when it exceeds the value of 3.5×10^{-5} the flow becomes in structurally-coupled as is seen in Fig. 3. In structurally-coupled flows the orientations of velocity vectors of both phases are similar and this implies high turbulent flows in the bath surface. Consequently, most of the casters operate in the transition zone or in the structurally-uncoupled zone presented in Fig. 3. Through the examination of video recordings of the two-phase flow inside the SEN, bubbling flow conditions and annular flow conditions yield structurally-uncoupled and structurally-coupled flows in the mold, respectively. Hereinafter the term structurally-coupled and structurally-uncoupled correspond to annular and bubbly two-phase flows in the SEN. Then any of these definitions can be employed indistinctly in the rest of the text. Experimental observations indicated also that structurally coupled flows presented the typical double roll flow above and below the port level of the SEN.

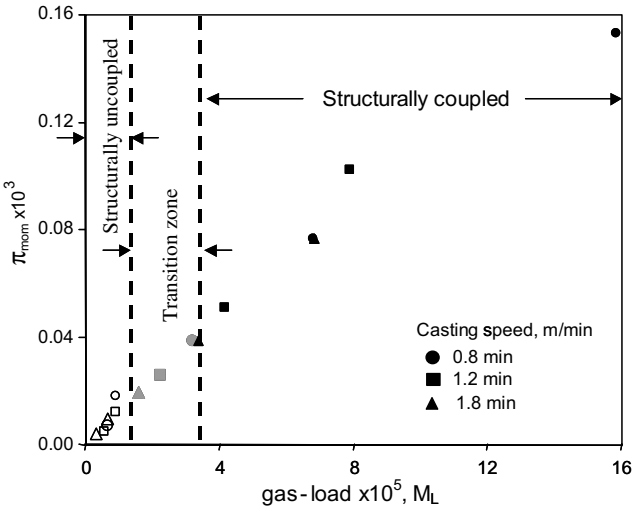

Fig. 3. Effect of gas-loads on the Π_{mom} at casting speeds of 0.8 m/s (80 l/min), 1.2 m/s (120 l/min) and 1.8 m/s (160 l/min).

3.2. Two-phase flows in the SEN

Fig. 4(a)–(f) show video images of the two-phase flow at 0.1, 0.2, 0.4, 0.7, 0.9 and 1.1 s respectively under a flow of 80 l/min of liquid and 0.5 l/min of gas (structurally uncoupled flow) taken at the middle section of the SEN body (mass load of 6.23×10^{-7}). A large bubble is formed at the injection point of air which elongates as the time passes on. After 0.7 s the bubble is so large that is not able to sustain the inertial forces of the liquid and suffers a breakup process forming smaller bubbles that flow downwards through the SEN length. At longer times, larger than 1.1–1.4 s, a new bubble is formed and the cycle repeats the process described. The effects of bubble formation and its further breakup has profound effects on liquid flow in the SEN well as is seen through the simulated velocity fields in the symmetrical plane which is perpendicular to the SEN's exit ports as is shown in Fig. 5(a)–(f) for the same times of 0.1, 0.2, 0.4, 0.7, 0.9 and 1.1 s, respectively with the same gas load (mathematical simulation of the two-phase flow in the well was preferred over direct video analysis due to experimental problems). At the beginning this structurally uncoupled flow seems to be symmetrical obeying a plug flow type and is well balanced regarding both exit ports (Fig. 5(a)–(c)); in the well the fluid observes small velocities. However, as the time passes on, after 0.7 s in Fig. 5(d), flow leaves the plug flow pattern becoming biased. Biasness starts just a time when the first bubbles, from a large broken up bubble, reaches the lower part of the SEN as is seen in Fig. 5(d). In the well of the SEN the fluid observes larger motions, as is seen in Fig. 5(g)–(j) when bubbles are already in contact with this containment. At end of the breakup process of a large bubble the flow is clearly biased at both ports as is seen in Fig. 5(j) where is seen that the two-phase jet has a downward angle in the left port and a near horizontal jet in the right port.

Effects of breakup processes of gas bubbles are particularly more evident in the vertical-symmetric plane which is parallel to both ports as is observed in Fig. 6(a)–(j) for times of 0.1, 0.2, 0.4, 0.7, 0.9, 1.1, 1.3, 1.5 1.6 and 2 s, respectively. At short times, Fig. 6(a)–(c), a planar front

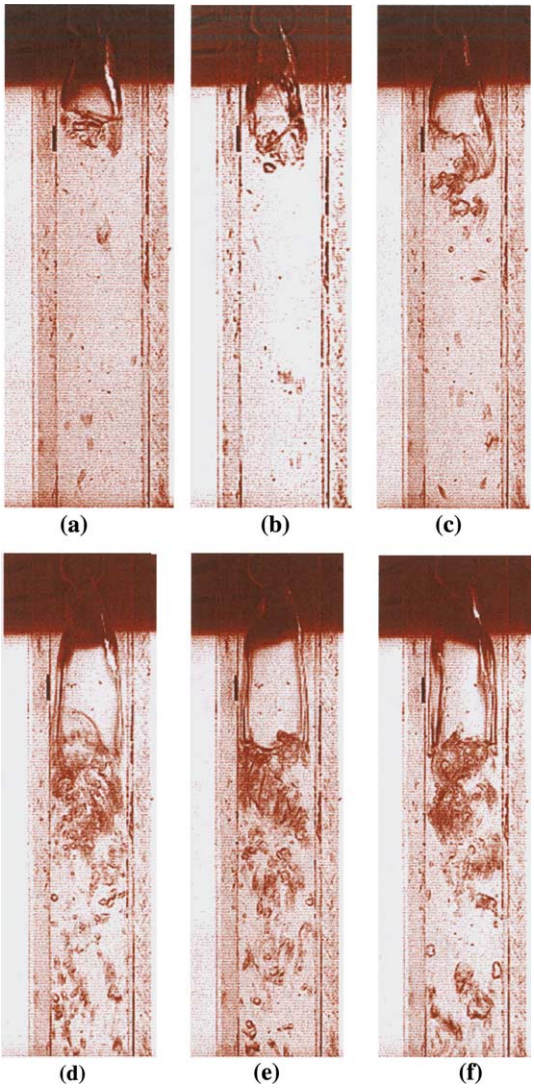

Fig. 4. Video images of the two-phase flow in the SEN at (a) 0.1, (b) 0.2, (c) 0.4, (d) 0.7, (e) 0.9 and (f) 1.1 s, respectively, at casting speed of 0.8 m/min and gas flow rate of 8.33×10^{-6} m^3/s.

of velocity vectors reaches the bottom of the SEN. Many velocity vectors, in the lower part of the SEN, are represented by dots because the fluid is coming out from a plane parallel to this page, toward the port exit. Again, after 0.7 s in Fig. 6(d), the flow is twisted and a strong recirculating flow in the well is rapidly formed and developed through the time as is seen in Fig. 6(e)–(j). These changes of flow patterns are responsible for the biased outflow through both ports of the SEN and they are originated by the presence of bubbles in the well.

Two-phase flow dynamics can be also visualized through the distribution of gas volume fractions inside the SEN, Fig. 7(a)–(f) show those distributions for times of 0.1, 0.2, 0.4, 0.7, 0.9,

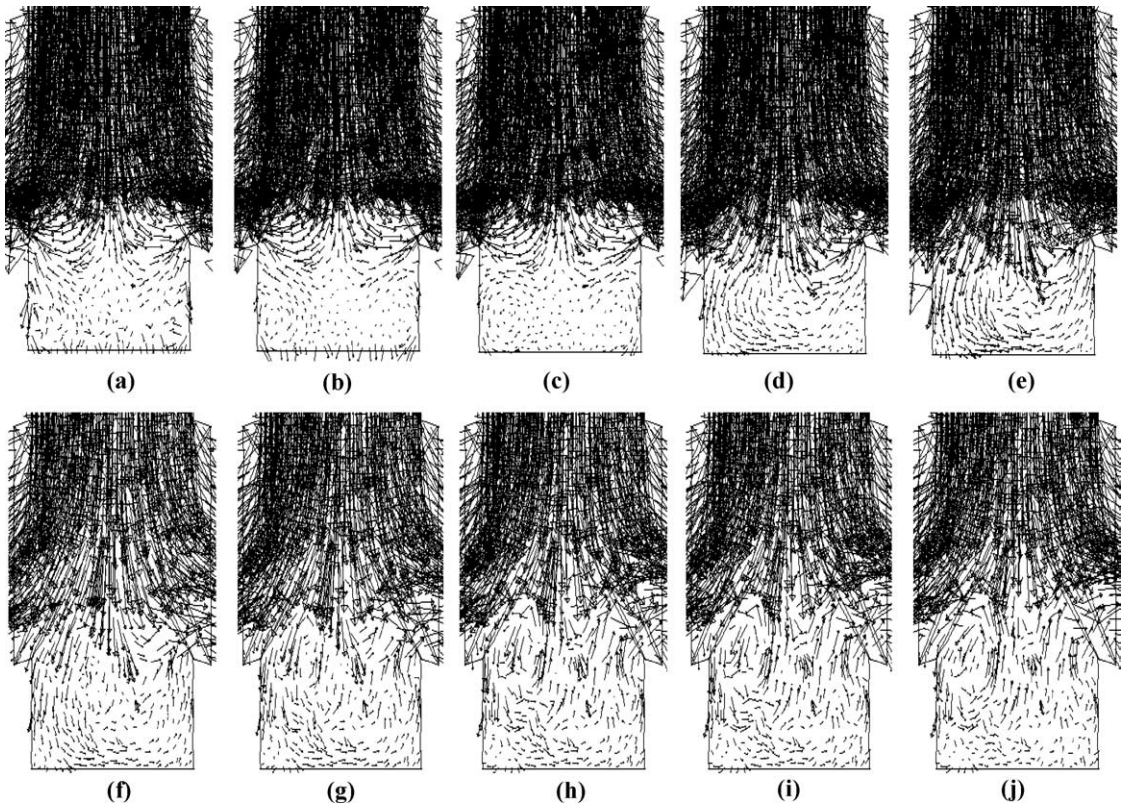

Fig. 5. Prediction of unsteady velocity fields at the perpendicular plane to both exit ports of the SEN at (a) 0.1, (b) 0.2, (c) 0.4, (d) 0.7, (e) 0.9, (f) 1.1, (g) 1.3, (h) 1.5, (i) 1.6 and (j) 2 s.

and 1.1 s, respectively. At times, such as 0.2–0.9 s, the large bubble suffers breakup process, as is indicated by the volume fractions of the gas phase, until it disappears completely at the time of 1.1 s to start a new cycle. This is in complete qualitative agreement with the images presented in Fig. 4(a)–(f). It is also noteworthy to mention that gas distribution inside the SEN is not symmetrical and this is another reason to the existence of biased flows through both ports of the SEN. When the gas load increases the cycles of the two-phase flow described above increase in frequency and the full column is filled with bubbles under breakup processes. Nevertheless, it should be acknowledged that the mathematical simulations are not able to predict accurately and quantitatively the complex two-phase flow but certainly provide a good qualitative description of the phenomena involved. Simulations with 80 l/min of water and 1.2 l/min of air are presented in Fig. 8(a)–(l). Main differences with the precedent case are that bubbles fill the full SEN length and that at the well the volume fraction of gas remains practically constant close to 30%. Thus gas is working as a cushion of the liquid impacting in the well producing a large amount of bubbles exiting toward the mold.

At the beginning of this cycle, as is shown in Fig. 8(a), gas volume fraction, according to the mathematical simulations, reaches a value close to 47% at the gas-inlet level. After a short time

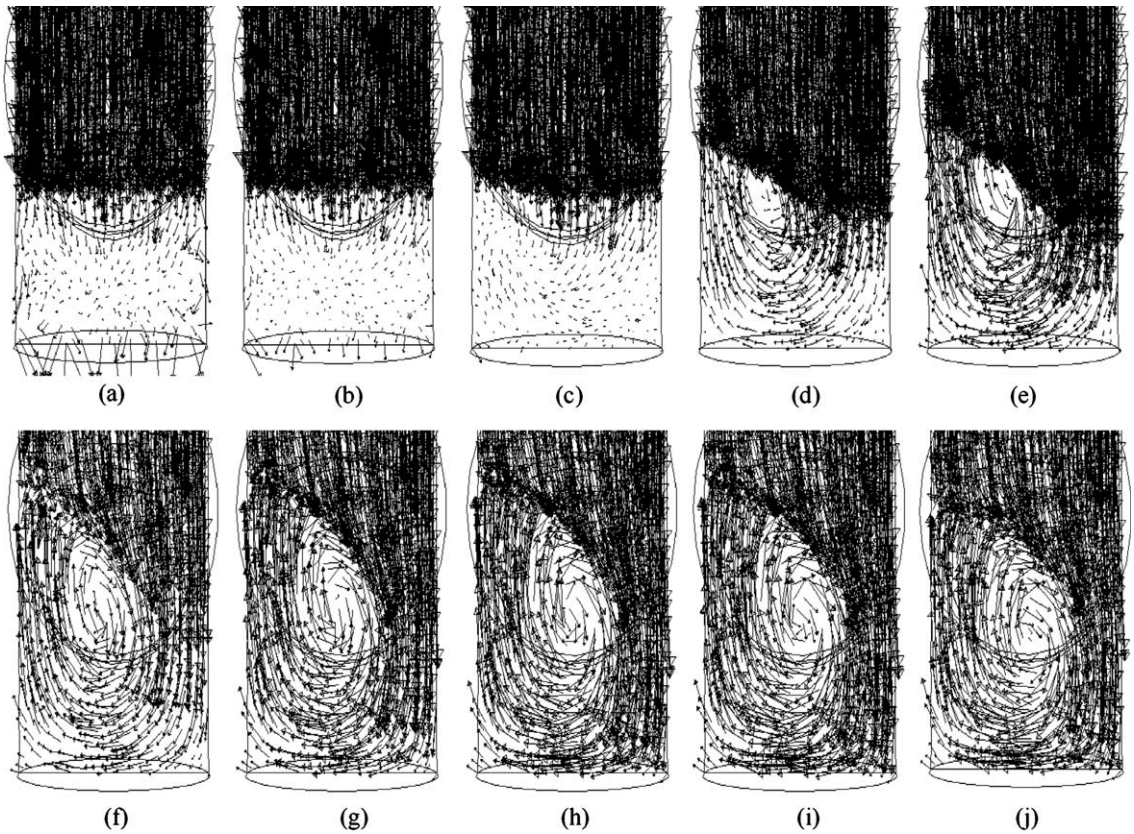

Fig. 6. Prediction of unsteady velocity fields at the parallel plane to both exit ports of the SEN at (a) 0.1, (b) 0.2. (c) 0.4, (d) 0.7, (e) 0.9, (f) 1.1, (g) 1.3, (h) 1.5, (i) 1.6 and (j) 2 s.

the volume fraction decreases to 4% at approximately half the SEN's height and increases again to about 19% at a point close to the ports. This sequence of events indicates that the liquid descends, through the SEN, following still a bubbling pattern. Further developments with time indicate that the two-phase column becomes richer of gas in its lower part, in the well, as indicated by the sequence of Fig. 8(b)–(g); the latter figure shows that the distribution of the volume fraction of the gas phase along the SEN is practically homogeneous. In Fig. 8(h), the concentration of gas in the SEN well reaches the highest value and decreases later, as is seen in Fig. 8(i)–(k) and decreases further as is seen in Fig. 8(l) to start again another cycle. When the two-phase flow in the SEN is bubbly flow exits from the SEN port by discontinuous torrents and the formation of one of them is observed in the sequence of Fig. 9(a)–(e). The flow of gas decreases as is shown in Fig. 9(f), to repeat another cycle just corresponding to the cycles described for the SEN according to the mathematical simulations. Then apparently gas is accumulated during a short time in the well and when it reaches a critical volume fraction, probably about 30% in the well, is suddenly expulsed by the liquid phase forming what we call here as torrent flows.

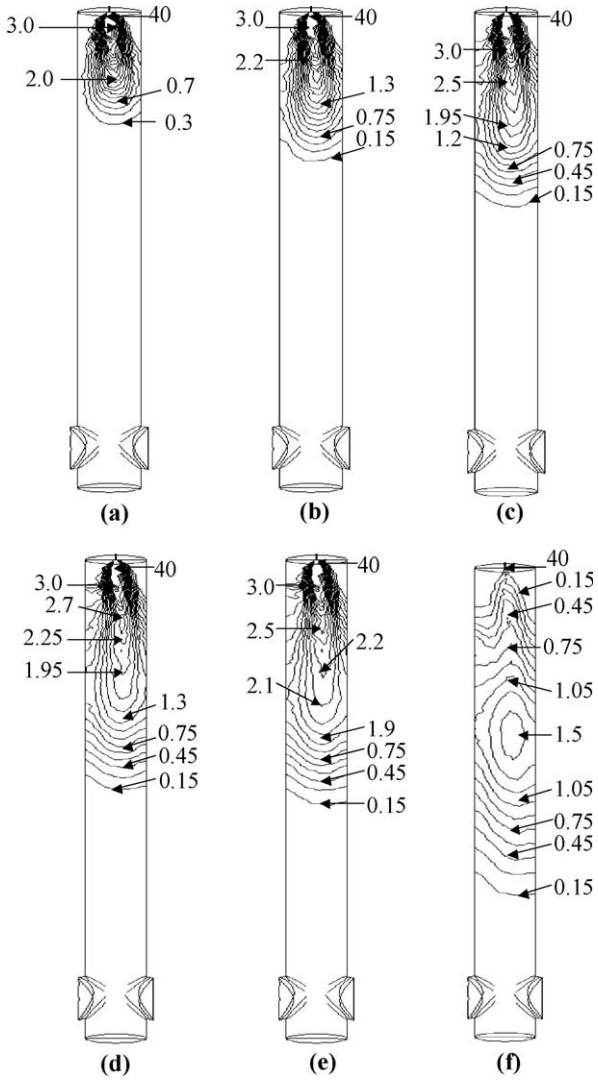

Fig. 7. Volume fractions $\times 10^{-2}$ of air with gas flow rate of 8.33×10^{-6} m^3/s (0.5 l/min) and casting speed of 0.014 m/s (80 l/min). (a) 0.1, (b) 0.2, (c) 0.4, (d) 0.7, (e) 0.9 and (f) 1.1 s.

3.3. Two-phase flows in the mold

Bubbles accumulated in the well of the SEN are shear strained and broken down by the well and the edges of the SEN ports and get out, forming smaller bubbles, together with the liquid entraining other bubbles, from the SEN toward the mold. Once in the mold bubbles suffer coalescence-breakup processes whose kinetics will depend basically on the gas load and probably from the initial size distribution of bubbles at the port. Here it is noteworthy again to comment that the term coalescence of bubbles can be actually be either of two phenomena; coalescence and agglomeration of bubbles, or both, since the image analyzer does not make a clear distinction

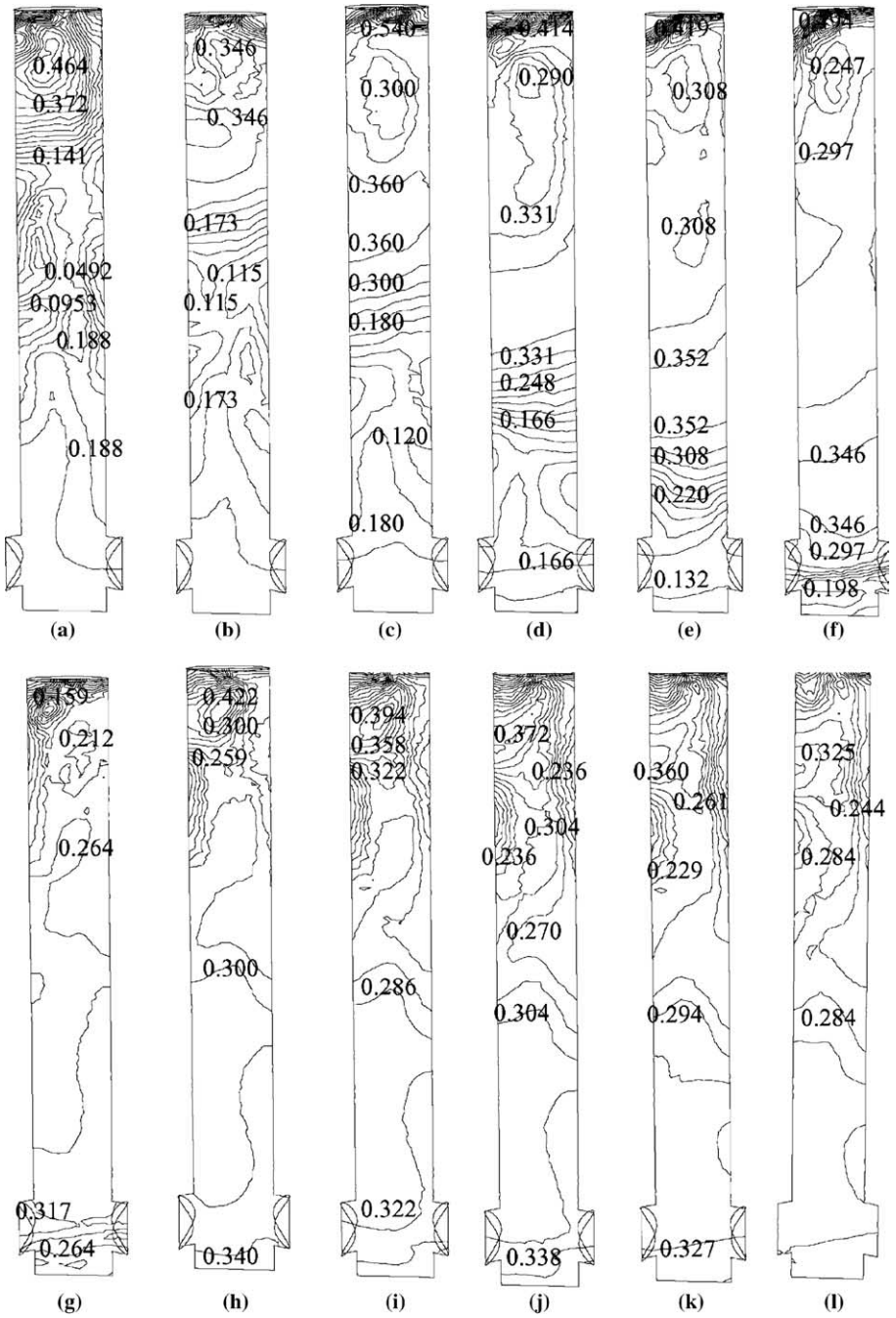

Fig. 8. Volume fractions of air with injection of gas flow rate of 2.0×10^{-5} m^3/s (1.2 l/min) and casting speed of 0.014 m/s (80 l/min). (a) 1, (b) 2, (c) 3, (d) 4, (e) 6.5, (f) 8, (g) 11, (h) 12.5, (i) 13, (j) 13.5, (k) 14.5 and (l) 15 s.

between them. Similarly, when we talk about bubbles breakup processes is probably that what is interpreted as such can be also related with the fast ascending of large bubbles leaving small bub-

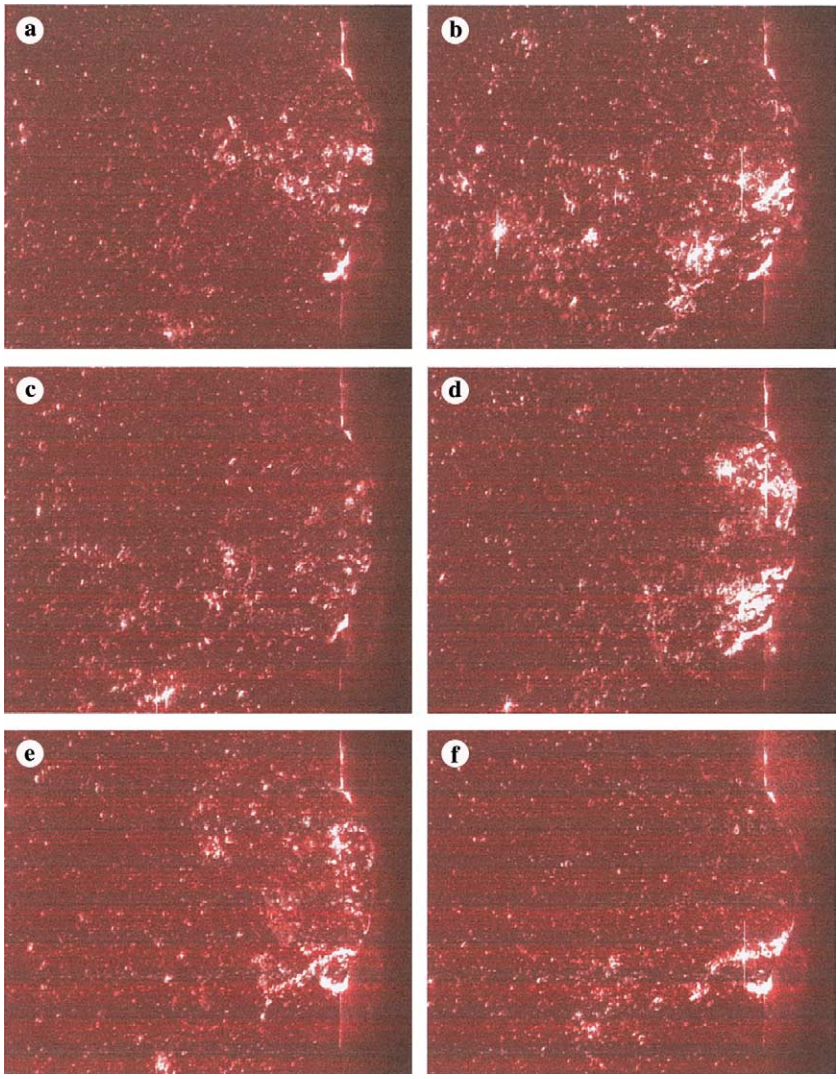

Fig. 9. Flow patterns of two-phase jets with injection of a gas flow rate of 2.0×10^{-5} m^3/s (1.2 l/min) and casting speed of 0.02 m/s (120 l/min).

bles in the field view of the CCD. Consequently terms, coalescence and breakup of bubbles must be understood with caution. In practical grounds the consequent effects of whether bubbles grow or agglomerate on the flow field must be macroscopically the same.

Although not determined quantitatively the bubbly-annular flow transition in the SEN was estimated, through visual observations, approximately at a gas load of 3×10^{-5}, which is the upper bound for structurally-coupled flows in the mold. Naturally this transition changes radically the flow pattern in the mold. Then when the flow becomes annular in the SEN, (or structurally coupled in the mold), a gaseous layer is formed all along the interior wall surface of the SEN, as was already mentioned above. Under these conditions the full cross section of the port is occu-

pied by the two-phase mixture exiting toward the mold as is seen in Fig. 10(a)–(f). Large bubbles are formed which ascend rapidly toward the bath surface (see Fig. 10(a)–(f)) and a great number of small bubbles are formed which will suffer coalescence-breakup processes during their travel from the SEN to, either, the bath surface or to the mold walls and later, eventually to the mold exit. These conditions correspond to a structurally coupled flow where both phases, gas and liquid, will follow similar path lines in the mold.

To analyze deeply the coalescence-breakup phenomena of bubbles a half width of this mold was arbitrarily divided into four zones as is shown in Fig. 11. The first zone is adjacent to the SEN and

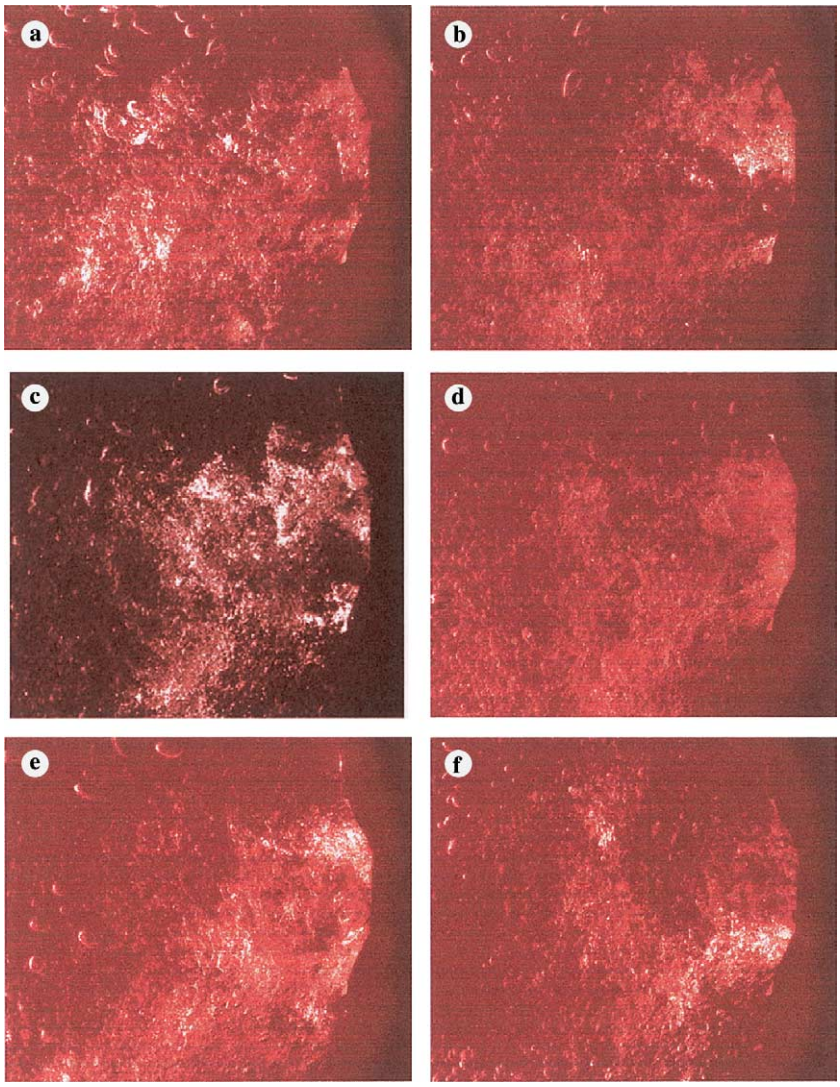

Fig. 10. Flow patterns of two-phase jets with injection of a gas flow rate of 1.67×10^{-4} m^3/s (10 l/min) and casting speed of 0.03 m/s (160 l/min), structurally-uncoupled flow.

the fourth one is close to the narrow wall of the mold. Effects of gas load in the four zones for casting speeds of 0.8, 1.2 and 1.8 m/min on bubbles population (calculated by dividing the number of bubbles in an average frame between the area of each zone presented in Fig. 11) are shown in Fig. 12(a)–(c), respectively. At low gas loads and low casting speeds (bubbly flows), Fig. 12(a), gas

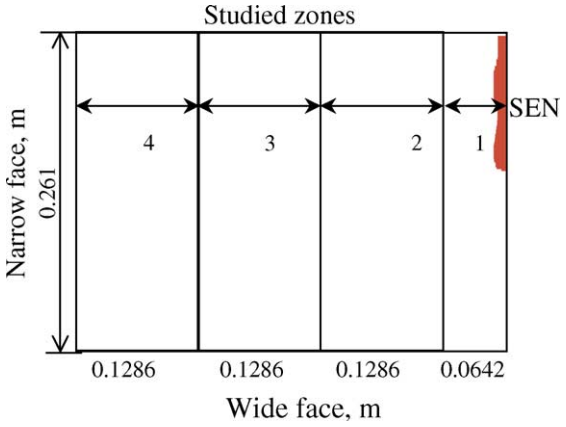

Fig. 11. Scheme of the four studied zones.

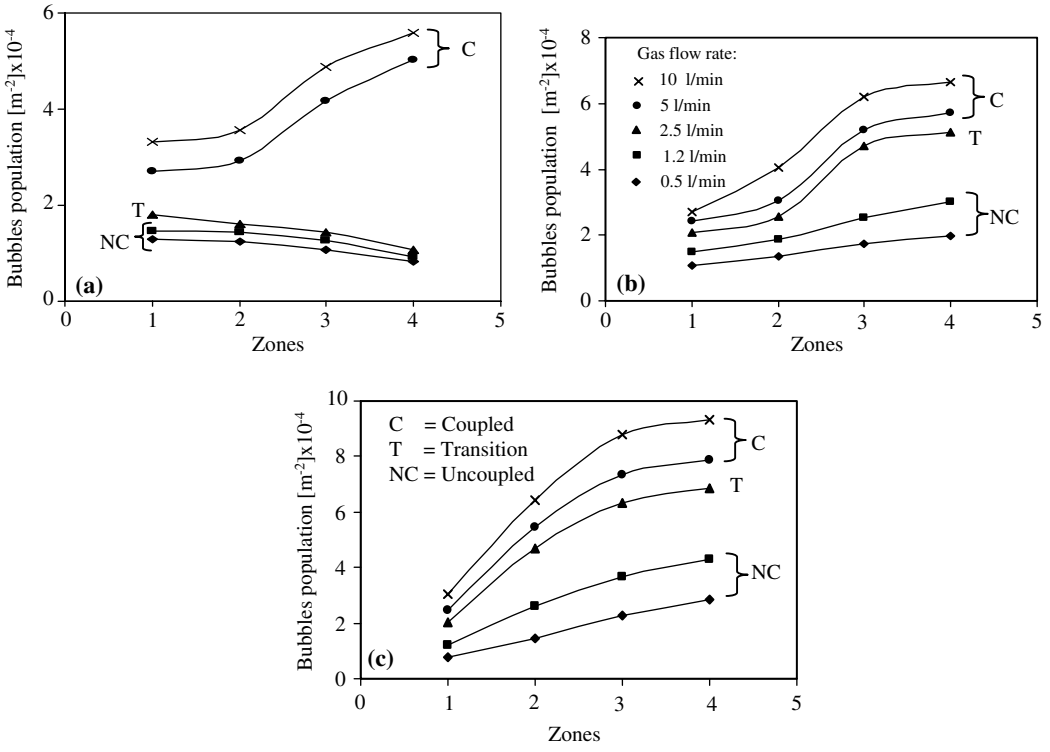

Fig. 12. Bubbles population per area at casting speeds of (a) 0.8, (b) 1.2 and (c) 1.8 m/min.

bubbles population show a maximum at zone 1, just in front of the port, to decrease at zones 2, 3 and 4. Flows are essentially uncoupled (marked with letters NC) or transition type as much (marked with letter T). The fact that the bubbles population remains practically constant indicates that they do not suffer further breakup processes since they are already small and the amount of energy necessary for that would be higher than that provided by the kinetic energy of the liquid phase. Then the sizes of the bubbles are very similar from the exit port until the narrow wall. At higher gas loads (annular flow in the SEN) bubbles population grows due to the higher amount of bubbles entrained by the liquid in flow field and the flow becomes structurally coupled (marked with letter C in Fig. 12(a)). Thus at a low casting speed structurally coupled flows lead to increase of the number of bubbles while transition and structurally uncoupled flows lead to a constant bubbles population or to a near constant population. At higher casting speeds and for any gas flow rate population of bubbles grows from the port until the narrow wall of the mold (see Fig. 12(b) and (c)). As would be expected, population growths are higher for structurally-coupled flows than for structurally-uncoupled or transition flows. High casting speeds will always increase the bubbles population from zone 1 to zone 4 indicating that the number of bubbles is high close to the narrow wall of the mold. From a practical standpoint a coupled flow would carry a great amount of bubbles to the shell–melt interface some of which would be trapped there.

Bubbles sizes follow a complex behavior at low gas loads and low casting speeds as is shown in Fig. 13(a) for a casting speed of 0.8 m/min corresponding to structurally uncoupled flows. Maxi-

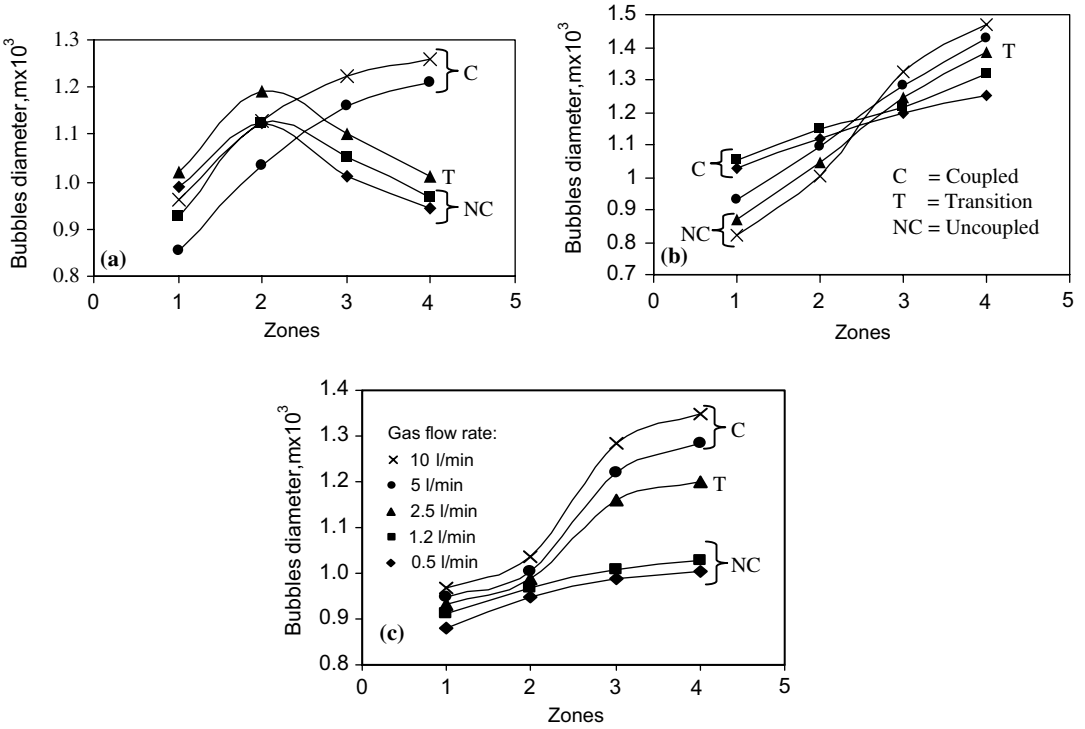

Fig. 13. Bubbles diameters at casting speeds of (a) 0.8, (b) 1.2 and (c) 1.8 m/min.

mum bubble sizes are observed at zone 2 and breaking up processes dominates at zones 3 and 4. At the lowest casting speeds (structurally-uncoupled) bubbles sizes increase at zones 1 and 2 due to coalescing processes (or what is interpreted here as such), and as a result of the nature of the two-phase flow inside the SEN. That is, the gas phase is accumulated in the well and flows together with the liquid forming a torrent type flow with large size bubbles close to the port. However, further in the mold, drag forces breakup those large bubbles or split agglomerated bubbles (this mechanism can be also applicable to transition flows at low casting speeds). At higher casting speeds and low gas flow rates (lowest gas loads) the mixture exits form the SEN through an intermittent two-phase jet mechanism as is seen in Fig. 14(a). Further in the mold, closer to the narrow wall bubbles concentrations decrease diminishing inter-bubble interactions and coalescence levels off.

At high casting speeds with high gas flow rate the mixture exits from the SEN through a continuous two-phase jet as is seen in Fig. 14(b). A continuous coalescence of bubbles from the port to the narrow wall is observed because bubbles concentrations steadily increase promoting intensive inter-bubble interactions and consequently favoring these processes.

At high casting speeds and low gas flow rates (structurally-uncoupled) the population of bubbles in the field is small (see Fig. 12(b) and (c)) and the inter-bubble interaction, as another result,

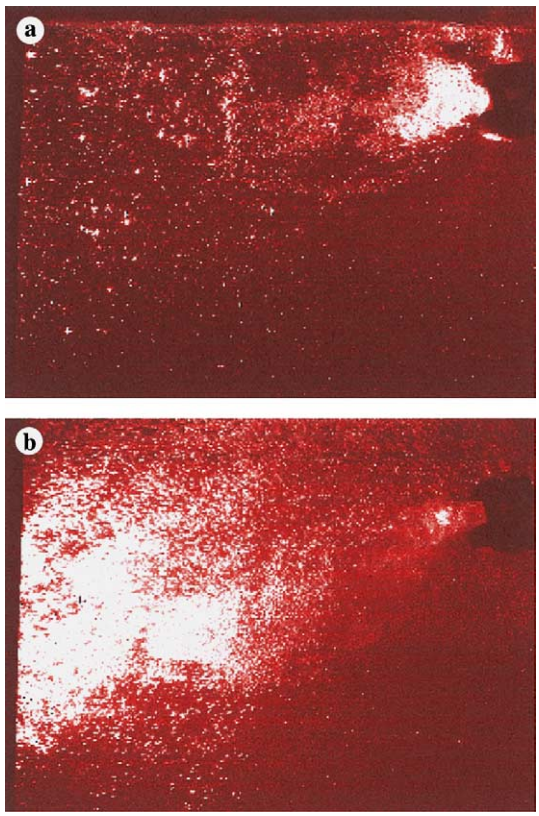

Fig. 14. Flow patterns of two-phase jets with injection of a gas flow rate of 1.67×10^{-4} m^3/s: (a) casting speed of 0.8 m/min (structurally-coupled flow) and (b) casting speed of 1.8 m/min (structurally-coupled flow).

is less frequent. The bubble growth is smaller due to smaller coalescence rate that increases also steadily from the SEN to the narrow wall where there is the highest bubbles population.

Annular flows in the SEN or structurally-coupled flows in the mold also led to high oscillations of the bath level; a lot of bubbles are dragged in the liquid bulk and great volumes of water are entrained by bubbles toward the top surface of the bath forming a foam layer. These conditions are unsuitable for a steady and safe operation of the actual mold. At high casting speeds is clear that there are coalescence processes of bubbles even for transition and structurally uncoupled flows. Naturally structurally coupled flows due to the reasons explained above, always yield larger bubbles close to the narrow wall than structurally-uncoupled flows.

The presence of gas affects radically the fluid flow of the liquid phase as can be seen, in velocity vector-fields (determined by PIV measurements by averaging 100 images), of Fig. 15(a) and (b) for a mono-phase flow of water with a flow rate of 160 l/min and for a two-phase, structurally-uncoupled, flow with the same flow rate of liquid and with a flow rate of gas of 1.2 l/min, respectively. In Fig. 15(a) a vortex is observed in the upper zone of the SEN port (1), another vortex located on

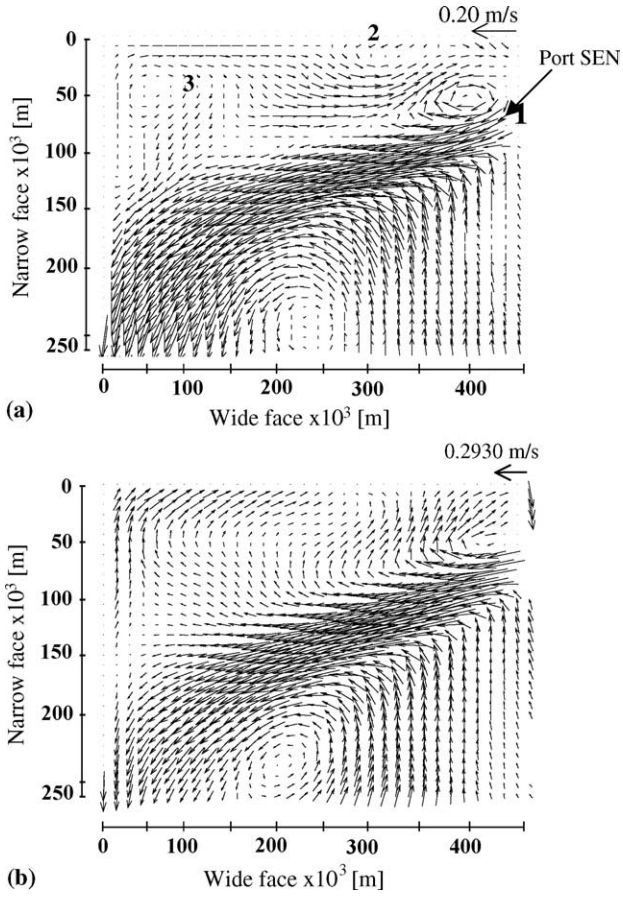

Fig. 15. Velocity vectors determined by the PIV of (a) mono-phase flow of water and (b) liquid velocities in the two-phase jets with injection of a gas flow rate of 2.0×10^{-5} m^3/s with casting speed of 1.8 m/min.

the bath surface close to the SEN (2) and a third one (3), with smaller dimensions, close to the upper left corner. In a two-phase flow (Fig. 15(b)) is seen that this small gas load is good enough to eliminate the presence of vortexes on the surface and close to the corner and decreases that above the port due to the presence of high buoyancy forces promoted by the ascending bubbles. This is a positive result because vortexes are responsible to promote flux entrainment into the liquid bulk forming macro inclusions in the solidified steel slab. This important result leads to conclude that structurally uncoupled of transition flows can be useful not only to avoid SEN clogging but to eliminate harmful vortexes from the flow.

Fig. 16(a) and (b) shows the corresponding velocity field and vorticity map of the gas phase corresponding to Fig. 15(b) for the two-phase flow. First of all, we can observe the similarity between velocity fields of both phases by comparing Fig. 16(a) with Fig. 15(a).

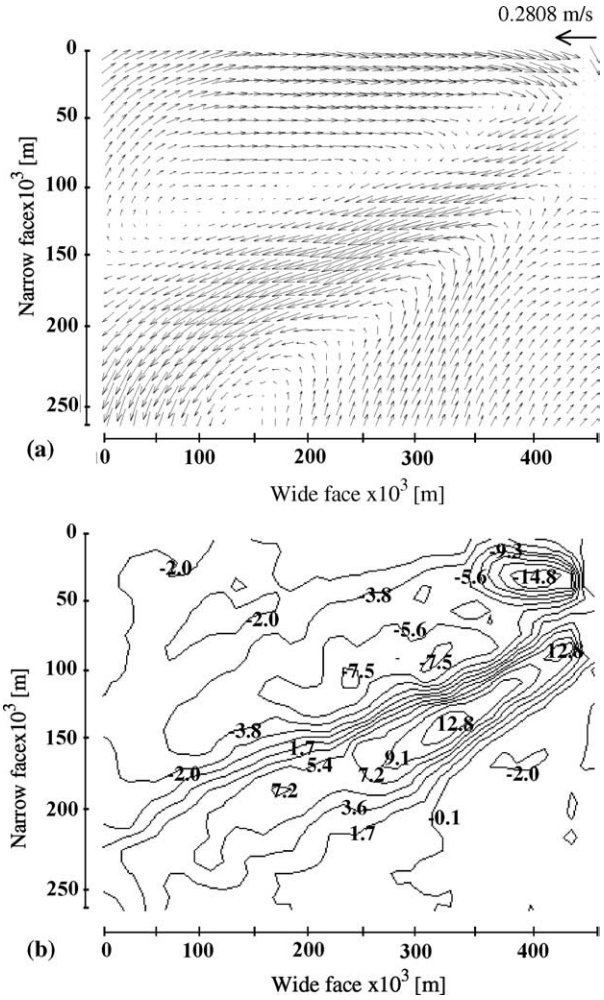

Fig. 16. Velocity field and vorticity maps of the gas phase jet with injection of a gas flow rate of 2.0×10^{-5} m^3/s with casting speed of 1.8 m/min.

After this study it is clear that the two-phase flow conditions in the SEN govern the two-phase flow patterns in the mold. Annular flows may be useful to unclog the exit ports but at expenses of unstable conditions. Since population of bubbles in structural-coupled flows is higher than the bubbles population in structural-uncoupled flows close to the narrow wall of the mold severe trapping conditions by the shell must be expected. Bubbly flows are safer in the sense that they promote more stable operating conditions of the mold avoiding excessive dragging and entrainment of bubbles by the liquid. However, they are less effective to solve problems of a clogged SEN, see Fig. 9(a)–(f). A practical suggestion to operate argon flow in molds is to use flows over the transition regime during short times exclusively to avoid SEN clogging.

Evidently the authors do not claim that all results and their description reported in this work are directly applicable to an actual continuous casting mold of steel slab, especially when the non-wetting condition at the solid liquid interface was not met. However, certainly the information found here provides a qualitative behavior of the actual two-phase flow in the system. Moreover, the present results represent a bottom line for future research where the non-wetting characteristics of the real system will be considered.

4. Conclusions

Two-phase flows in the submerged entry nozzle of a continuous casting slab mold and its influence on the two-phase flows in the mold have been studied using video recording, mathematical simulations and particle image velocimetry techniques and the conclusions derived are as follows:

1. Bubbly and annular flows in the SEN are directly related with structurally-uncoupled and structurally coupled-flows in the mold, respectively.
2. Under bubbling conditions in the SEN the presence of bubbles promote periodical twisting motions of liquid stream inside the SEN well and consequently liquid flow is biased through both exit ports.
3. Mathematical simulations of two-phase, bubbly flows, predict qualitatively the experimental observations made through a video recording technique.
4. Population and sizes of bubbles in the mold increase with higher gas loads and increases of casting speeds under structurally coupled conditions.
5. The presence of a gas flow, even at small volume fractions, eliminates the presence of vortexes observed in mono-phase flows of liquid due to the alteration of shear strains of the liquid shearing flow in the mold.

Acknowledgements

The authors give the thanks to the institutions COFAA, CoNaCyT and SNI for the financial support to the Group of Mathematical Simulation of Materials Processing and Fluid Dynamics of ESIQIE-IPN.

References

Bai, H., Thomas, B.G., 2001a. Turbulent flow of liquid steel and argon bubbles in slide-gate tundish nozzles: Part I. Model developments and validation. Metall. Mater. Trans. B. 32, 253–267.

Bai, H., Thomas, B.G., 2001b. Turbulent flow of liquid steel and argon bubbles in slide-gate tundish nozzles: Part II. Effect of operation conditions and nozzle design. Metall. Mater. Trans. B 32, 269–283.

Bai, H., Thomas, B.G., 2001c. Effects of clogging, argon injection, and continuous casting conditions on flow and air aspiration in submerged entry nozzles. Metall. Mater. Trans. B 32, 707–722.

Bai, H., Thomas, B.G., 2001d. Bubble formation during horizontal gas injection into downward-flowing liquid. Metall. Mater. Trans. B. 32, 1143–1159.

Burty, M., Larrecq, M., Pusse, C., Zbacyniak, Y., 1995. Experimental and theoretical analysis of gas and metal flows in submerged entry nozzles in continuous casting, In: 13th PTD Conference Proc., Iron and Steel Society, pp. 287–291.

Chung, T., 2002. Computer Fluid Dynamics. Cambridge University Press, Cambridge, London, New York, NY.

Hirt, C.W., Nichols, B.D., 1981. Volume of fluid (VOF) method for the dynamics of free boundaries. J. Comput. Phys. 39, 201–225.

Hoffmann, K.A., 1989. Computational Fluid Dynamics for Engineers. The University of Texas at Austin Press, Austin, TX.

Ishiguro, K., Iguchi, M., 2003. Model experiment of the behavior of argon gas in immersion nozzle. ISIJ Int. 43, 663–670.

Launder, B.E., Spalding, D.B., 1974. Comput. Methods Appl. Mech. Eng. 3, 269–289.

Mizuno, Y., Iguchi, M., 2001. Behavior of bubbles attaching and detaching from solid body of poor wetability. ISIJ Int. 41, S56–S60.

Odenthal, H.J., Lemanowics, I., Goriseen, R., Pfeifer, H., 2002. Simulation of submerged entry nozzle-mold water model system using laser-optical and computational fluid dynamics. Metall. Mater. Trans. B. 33, 163–172.

Sánchez-Pérez, R., Morales, R.D., Díaz-Cruz, M., Olivares-Xometl, 2003. A physical model for the two-phase flow in a continuous casting mold. ISIJ Int. 43, 637–646.

Sánchez-Pérez, R., Morales, R.D., García-Demedices, L., Palafox-Ramos, J., Díaz-Cruz, M., 2004. Dynamics of coupled and uncoupled two-phase flows in a slab mold. Metall. Mater. Trans. B. 35, 85–99.

Thomas, B.G., Zhang, L., 2001. Mathematical modeling of fluid flow in continuous casting. ISIJ Int. 41, 1181–1193.

Thomas, B.G., Denissov, A., Bai, H., 1997. Behavior of argon bubbles during continuous casting of steel, In: 80th Steelmaking Conf. Proc., Iron and Steel Society, pp. 375–384.

Wang, Z., Mukai, K., Ma, Z., Nishi, M., Tsukamoto, H., Shi, F., 1999. Influence of injected Ar gas on the involvement of mold powder under different wetabilities between porous refractory and molten steel. ISIJ Int. 39, 795–803.

Yokoya, S., Takagi, S., Iguchi, M., Asaki, Y., Westoff, R., Hara, S., 1998. Swirling effect in immersion on flow and heat transport in billet continuous casting mold. ISIJ Int. 38, 827–833.

Yokoya, S., Takagi, S., Iguchi, M., Marukawa, K., Yasugaira, W., Hara, S., 2000a. Development of swirling flow generator in immersion nozzle. ISIJ Int. 40, 548–588.

Yokoya, S., Takagi, S., Iguchi, M., Marukawa, K., Hara, S., 2000b. Swirling flow effect in immersion nozzle on flow in slab continuous casting mold. ISIJ Int. 40, 578–583.

Yokoya, S., Takagi, S., Iguchi, M., Marukawa, K., Hara, S., 2001. Swirling flow control in immersion nozzle for continuous casting process. ISIJ Int. 41, S47–S51.

Yuan, Q., Thomas, B.G., Vanka, S.P., 2003. Turbulent flow and particle motion in continuous slab casting molds. ISSTech 2003, 913–927.